Transient Liquid Phase Spark Plasma Sintering of B_4C-based Ceramics using Ti-Al Intermetallics as Sintering Aid

Wei Ji [1, 2], Richard I Todd [2], Weimin Wang[1], Hao Wang[1], Jinyong Zhang[1], Zhengyi Fu[*1]

1. State Key Laboratory of Advanced Technology for Materials Synthesis and Processing, Wuhan University of Technology,122 Luoshi Road, Wuhan 430070, China.

2. Department of Materials, University of Oxford, Parks Road, Oxford OX1 3PH, UK.

Abstract:

Fully-dense B_4C-based ceramics were fabricated using Ti-Al intermetallics as sintering aid by Spark Plasma Sintering at a low temperature of 1700 °C whilst applying 32 MPa uniaxial pressure. The influence of the intermetallic additions on the phase composition, morphology and mechanical properties of the ceramics were investigated. The intermetallics flowed and react with B_4C to form a three-phase composite containing B_4C, TiB_2 and Al_4C_3 during the transient liquid phase sintering process. The TiB_2 and Al_4C_3 particles were located on the boundaries between B_4C grains and effectively inhibited the growth of B_4C, which improved the mechanical properties. Good bonding between B_4C and the phases formed was confirmed by TEM analysis. The specimens with 5 wt. % Ti-Al provide an attractive combination of homogeneous morphology and excellent mechanical properties, including a Vickers hardness of 33.5±0.4 GPa, a flexural strength of 506±16 MPa and a fracture toughness of 5.5±0.1 $MPa \cdot m^{0.5}$.

Keywords: Boron Carbide; Ti-Al intermetallics; spark plasma sintering; transient liquid phase; mechanical properties

* Corresponding author: Tel.: +86 027 87865484; Fax: +86 027 87215421;
E-mail address: zyfu@whut.edu.cn

1. Introduction

Boron Carbide (B_4C) has attracted considerable attention because of its attractive combination of properties, including high hardness (the third hardest substance), low density (one of the lightest ceramic), high elastic modulus, high melting point (2450 °C), excellent chemical stability and high neutron absorption cross section. These properties make it a fascinating material for various applications, such as light-weight armors, cutting tools, wear-resistant parts and neutron radiation absorbent in nuclear reactors **[1,2,3]**. However, the applications of monolithic B_4C are limited due to the difficulties in obtaining highly dense bulk materials even by pressure-assisted sintering methods. Its strong covalent bonding, low self-diffusion coefficient and oxygen-rich-layer (mainly B_2O_3) covered surface are the main reasons that make it difficult to sinter.

To overcome these difficulties, two main methods have been used to improve the sinterability of B_4C. The first one is increasing the sintering temperature to higher than 2200 °C **[4]**, while the second one is using sintering additives, such as Al, Fe, Ti, Si, B, C, Al_2O_3, TiB_2 and Si_3C_4 .etc., to lower the sintering temperature **[5,6,7,8,9,10]**. The first method is inadvisable for energy conservation. Moreover, high sintering temperature leads to dramatic grain growth, which could reduce the strength **[11]**. The second method is usually used to fabricate B_4C-based composites. However, the density of the bulks increases remarkably compared with pure B_4C, which severely compromises the engineering applications for this light-weight material. Liquid phase sintering aids may also compromise the high temperature properties and hardness of

the ceramics.

Ti-Al intermetallics exhibit characteristics of both metals and ceramics and have been attracting more and more attention **[12,13]**. We suggest the relatively low melting point and low density of Ti-Al intermetallics favor the fabrication of dense and light-weight B_4C-based ceramics by liquid-phase sintering. In addition, the spark plasma sintering (SPS) has been confirmed in facilitating the densification of B_4C at low temperature **[14,15]**. In our present study, the influence of Ti-Al intermetallics as sintering additive on densification, phase composition, microstructure and mechanical properties of B_4C through the SPS route at low temperature with common uniaxial pressure were investigated. It is found that the Ti-Al intermetallics act as a transient liquid phase sintering aid which enables the potential retention of the refractory properties of B_4C.

2. Experiment procedures

Commercially available Boron Carbide (B_4C, Mudanjiang Diamond Boron Carbide Co., Ltd., China) and Titanium Aluminide (Ti-Al intermetallics, Alfa Aesar) were used as starting materials without further purification. According to the supplier data, a small amount of free carbon (< 1 wt. %) and B_2O_3 (< 0.2 wt. %) exists in the raw B_4C powder. The weight ratio of TiAl to Ti_3Al in Ti-Al intermetallics is approximate 9:1 according to Rietveld refinement. The average particle size of B_4C powder is 2.36 μm and the Ti-Al intermetallic powder is ~ 45 μm (both manufacturers' data). The morphology of the starting powders is shown in Fig.1. The powder mixtures of B_4C with different contents of Ti-Al intermetallics (0,1, 3, 5 and 7 wt. %)

were obtained by wet ball-milling(GMJ/B, Xianyang JinHong General Machinery Co., LTD, Xianyang, China) in polyethylene jars with agate balls and ethyl alcohol as media for 24 h. The slurry was dried in a rotary evaporator at 65 °C and granulated by a 200 mesh sieve. The B_4C-based ceramics were obtained by a Spark Plasma Sintering apparatus (SPS, Dr. Sinter-3.20MK II, Sumitomo Coal Mining Co. Ltd., Tokyo, Japan) using a cylindrical graphite die with an inner diameter of 20 mm, under a temperature of 1700 °C for 5 min with a uniaxial pressure of 32 MPa. The temperature was automatically raised by the SPS apparatus to 600 °C over a period of 3 min, and from this point and onwards it was monitored and regulated by an infrared thermometer focused on the surface of the die with a heating rate of 100 °C/min. The compaction pressure was applied above 600 °C and maintained during the rest of the heating and soaking time in the SPS. Natural cooling began when the power was turned off at the end of the soaking, and the applied uniaxial pressure was removed at the same time. During sintering, the die was wrapped with graphite wool for temperature homogeneity.

The crystal structure of the as-sintered specimen was characterized by X-ray diffraction (XRD, X'Pert PRO-PANalytical) with Cu Kα radiation. The specimens' surfaces were ground with a diamond wheel and polished to 0.25 μm to get mirror-finish surfaces for successive microstructure examinations. Polished and etched microstructures of the specimens with different contents of Ti-Al intermetallics were observed by scanning electron microscopy (SEM, Hitachi 3400), the electrolytic etching was performed in 1% KOH solution with a current density of 0.1 A/cm^2 for

20~30 s on the polished surfaces. The grain sizes of sintered B_4C samples were determined from the SEM images using the average of the length and width from at least 50 randomly selected grains. The elemental analysis of the samples was carried out by Electron Probe Microanalysis (EPMA, JEOL JXA-8230) equipped with Wavelength Dispersive Spectroscopy (WDS, Jeol-8230) and Energy Dispersive Spectrometer (EDS, Oxford Inca x-act). A thin foil of sintered material was prepared by mechanical thinning followed by ion milling and observed using transmission electron microscopy (TEM, JEOL JEM-2010HT) equipped with selected area electron diffraction (SAED) and high resolution transmission electron microscopy (HRTEM, JEOL JEM-2100F).

Specimens for mechanical testing were cut from the SPS-ed pellets. Each specimen was polished with diamond suspension down to 0.25 μm. The edges were chamfered to minimize stress concentration. The Vickers hardness was measured by a Vickers hardness tester (Wolpert-430SV) with applied load of 9.8 N for a dwell time of 15 s. Fracture toughness, K_{IC}, of the ceramics after the indentation was calculated using Eq. (1) as reported for B_4C in Ref. **[16]**.

$$K_{IC}=0.203\ H_v\ a^{1/2}\ (c/a)^{-3/2} \quad (1)$$

here H_v is the hardness, a is the impression radius, and c is the radial/median crack length. The flexural strength measurements were carried out via three point bending test on 2 mm×3 mm×18 mm bars in a ceramic test system (MTS 810, MTS) with a span of 15 mm at a crosshead speed of 0.5 mm/min. The reported values of relative density and mechanical properties are the average of at least ten measurements.

3. Results and discussion

X-ray diffraction patterns of B_4C ceramics with varying Ti-Al addition are shown in Fig.2. Only B_4C phase is detected in the pure B_4C sample. For specimens containing Ti-Al additions, peaks belong to TiB_2 can be identified. The intensity of TiB_2 increases with the elevated content of Ti-Al intermetallics. With the addition of 7 wt. %, a third phase, Al_4C_3, appears in the XRD patterns. The results indicate that B_4C reacts with Ti-Al additions during the sintering process to form ceramic phases. Possible reactions are proposed by Eq. (2) and Eq. (3) as:

$$6B_4C + 4Ti_3Al \rightarrow 12TiB_2 + Al_4C_3 + 3C \quad (2)$$

$$2B_4C + 4TiAl + C \rightarrow 4TiB_2 + Al_4C_3 \quad (3)$$

No free carbon or B_2O_3 were detected in the XRD patterns. This is because the free carbon from the raw materials or formed during reaction (2) can react with B_2O_3, thereby eliminating the B_2O_3 coating on B_4C particles **[17]**, and promoting the sinterability of B_4C.

$$2B_2O_3 + 7C \rightarrow B_4C + 6CO\uparrow \quad (4)$$

The microstructures of B_4C ceramics with different contents of Ti-Al intermetallics were examined by SEM of polished surfaces. As shown in Fig. 3(a), the pure B_4C specimen contains pores. But with the increase of Ti-Al sintering aids, the samples reach high relative density, which means the addition of Ti-Al dramatically decreased the residual porosity. The phase distribution in Fig. 3(b)-(d) shows that the second phase disperses homogeneously in the B_4C matrix. As the addition amount was increased to 7 wt. %, coarse second phase particles were formed, reducing the

uniformity. Three phases with different contrast can be observed on the polished surfaces. The dark phase is the B_4C matrix, and the other two phases are the products from the reaction between B_4C and Ti-Al intermetallics. The sizes of the formed phases are much smaller than that of raw Ti-Al particles (~ 45 μm), which suggests that the Ti-Al particles first melted during the process and then reacted with the B_4C at higher temperature. According to the Ti-Al phase diagram, the Ti-Al intermetallics should be fully molten by 1550 °C. The sintering can therefore be identified as transient liquid phase sintering. Compared with the results in Ref. **[18]** using the same raw B_4C powder (pure B_4C, SPS: 2050 °C/ 32 MPa/ 6 min, 98% relative density), the sintering temperature was lowered by 300 °C in our present work. At such a low temperature, it is a solid sintering system for the densification of pure B_4C, but when Ti-Al intermetallics are added to the B_4C, it becomes to a liquid-phase sintering system instead. The sintering is promoted essentially by the particle rearrangement due to the liquid flow and the solution-precipitation mechanism for mass transfer.

In order to reveal the grain morphology of B_4C based ceramics with different Ti-Al content, electrolytic etching was conducted as shown in Fig. 3 (f)-(j). The mean grain sizes of the B_4C-based ceramics with different Ti-Al content at 0 wt. %, 1 wt. %, 3 wt. %, 5 wt. %, and 7 wt. % are 2.4±0.2 μm, 2.5±0.4 μm, 2.5±0.4 μm, 2.4±0.3 μm, and 3.5±1.4 μm, respectively. In the sintering process, densification and grain growth are two competing mechanisms. The activation energy for densification may be lower than that for grain growth in some systems **[19]**. Since 1700 °C is a very low temperature for the sintering of B_4C, which could not activate the grain growth [14],

the grain size of the pure B_4C bulk remained the same as for the raw materials, as seen in Fig. 3(f). When Ti-Al intermetallics were added to the B_4C, the second phases were located at the B_4C boundaries, which also inhibit the grain growth of B_4C. It is worth pointing out that the pores seen in Fig. 3(f)-(j) are the positions where the second phases were removed by the etching process since these are not seen in the unetched specimens (Fig. 3 (a)-(e)). With a Ti-Al content of 5 wt. %, fully dense B_4C ceramics almost without grain growth were obtained. Fig. 3(j) shows that the non-uniform distribution of particles identified in Fig. 3(e) and/or larger amounts of liquid phases formed on melting of the Ti-Al intermetallics in the 7 wt. % specimen also led to abnormal grain growth.

EPMA equipped with WDS and EDS was used to investigate the distribution of different elements (Ti, Al, B and C) of the sample with 7 wt. % Ti-Al addition. A region with phases of different contrast was chosen. The element mappings together with the original SEM micrograph are shown in Fig. 4. Fig. 4(a) - Fig. 4(d) reveal the distribution of Ti, Al, B and C, respectively. Combined with the XRD results and the SEM back scattered-electron image shown in Fig. 4(e), we conclude that the white phase is TiB_2 and the grey one is Al_4C_3, as expected from the atomic number of the elements involved. No Si or O was detected in the sample by element analysis showing that any contamination from the agate milling media was below the detection limit of the microanalysis.

TEM analysis was performed on the B_4C-based ceramic with 5 wt. % Ti-Al sintered at 1700 °C. Fig. 5 and Fig. 6 show the interface between B_4C and the two

different second phases. The SAED patterns in Fig. 5(a) indicate that the particle B surrounded by B_4C grains is TiB_2. The HRTEM image of the boundary in Fig. 5(b) shows a clean and narrow grain boundary between B_4C (d=0.378nm, (012) zone axis) and TiB_2 (d=0.323nm, (0001) zone axis) grains. The clean boundary suggests strong binding between B_4C and TiB_2. It is well known that the grain boundary strength between matrix and second phases has a significant effect on the properties of the composites, especially the mechanical properties. Therefore this suggests that excellent mechanical properties can be obtained for these ceramics. TEM images of B_4C and Al_4C_3 are shown in Fig. 6. Nano-sized particles of Al_4C_3 filled in the triple junction of B_4C grains. The region shape is very similar to liquid phase in cermet **[20]**. This unique structure confirms a transient liquid phase sintering mechanism for this sintering system. In addition, the straight grain boundaries of the triple junction indicate good physical compatibility between the two phases.

Fig.7 shows the density and relative density of the B_4C based ceramics with different contents of Ti-Al. The theoretical densities of the specimens were determined based on the rule of mixtures by assuming the complete conversion of Ti-Al into TiB_2 and Al_4C_3. It can be seen that only ~84.5% of the theoretical density can be obtained for the pure B_4C sintered at 1700 °C. The low density was mainly attributed to its poor sinterability of B_4C at low temperature. The relative densities of the samples increased remarkably as Ti-Al was added. With 5% Ti-Al content, the relative density reached 99.5%. No obvious change could be observed when the amount of Ti-Al was further increased. These results demonstrate that Ti-Al aid could

effectively improve the sintering behavior of B_4C. In addition, the density of the near fully dense B_4C-based ceramics is less than 2.55 g/cm^3, which well retains the advantage of light weight for B_4C-based material. Furthermore, the replacement of the low melting point Ti-Al intermetallics with the refractory phases TiB_2 and Al_4C_3 during transient liquid phase sintering can be expected to restore the high temperature properties of B_4C, thus removing the usual disadvantage of liquid phase sintering aids.

The effect of Ti-Al content on the mechanical properties of B_4C is shown in Fig.8. The flexural strength, fracture toughness and Vickers hardness of the pure B_4C were 210±13 MPa, 2.9±0.2 MPa·m$^{0.5}$ and 17.9±0.3 GPa, respectively. With the addition of 5 wt. % Ti-Al intermetallics, the values increased remarkably to 506±14 MPa, 5.5±0.1 MPa·m$^{0.5}$ and 33.5±0.4 GPa. Further increase of additive content had a negative influence on the properties.

The mechanical properties can be explained in terms of the variations in relative density and grain structure. The increments in flexural strength, fracture toughness and Vickers hardness are mainly attributed to the improvement of the relative density and the maintenance of grain size, compared with the pure B_4C. With further additions of Ti-Al, the flexural strength, fracture toughness and Vickers hardness decrease slightly due to the abnormal grain growth and the inhomogeneous distribution of the second phases, as shown in Fig. 3(e). The decrement of hardness is also related to the second phases (TiB_2 and Al_4C_3) with lower hardness.

Fig .9 shows the SEM images of the crack propagating after indentation on the polished surface of B_4C ceramics with different Ti-Al contents. As shown in Fig. 9(a),

the fracture mode of the specimen with 1 wt. % Ti-Al is predominantly transgranular. With the content of 3 wt. % and 5 wt. %, crack deflection and crack bridging can be observed. The change of fracture mode may be associated with the residual stress induced by the small particles located in the grain boundary. The large second phases in the 7 wt. % Ti-Al specimen exhibited multiple cracking which is also responsible for the slight degradation of mechanical properties seen.

A comparison of the properties of the B_4C-5 wt. % ceramic in the present work with other B_4C-based ceramics in the literature is shown in Table 1. For pure B_4C ceramics, a temperature of above 2000 °C is required for attaining high relative density by pressure-assisted sintering methods under a pressure of ~35 MPa. However, it is demonstrated by our work that fully dense B_4C-based ceramics with moderate grain growth can be fabricated at a lower temperature (1700 °C) under a commonly used pressure for spark plasma sintering by adding a small amount of sintering Ti-Al aid. In addition, the lightweight B_4C-based ceramics possess a better combination of dense microstructure, excellent mechanical properties and contain only high melting point phases after sintering.

4. Conclusion

Fully-dense B_4C-based ceramics with limited grain growth were successfully fabricated using 1, 3, 5 and 7 wt. % Ti-Al intermetallics as sintering aid, by SPS at temperature of 1700 °C and uniaxial pressure of 32 MPa for 5 min. During transient liquid phase sintering, the intermetallics first melt and promote sintering and then

react with B_4C to form a three-phase composite containing only the refractory phases B_4C, TiB_2 and Al_4C_3. The formation of nanosized or quasi-nanosized TiB_2 and Al_4C_3 particles effectively inhibits the grain growth of B_4C and improves the mechanical properties. The sample with 5 wt. % Ti-Al content provides an attractive combination of homogenous morphology and excellent mechanical properties, including a Vickers hardness of 33.5±0.4 GPa, a flexural strength of 506±14 MPa and a fracture toughness of 5.5±0.1 $MPa \cdot m^{0.5}$.

Acknowledgment

This work was financially supported by the National Natural Science Foundation of China (51521001) and the Ministry of Science and Technology of China (2015DFR50650). The authors also thank Mr. Xuefeng Ruan from School of Power and Mechanical Engineering of Wuhan University for the help in Spark Plasma Sintering, Prof. Rong Jiang, Prof. Yadong Sun and Ms. Tingting Luo from Materials Analysis Center of Wuhan University of Technology for their help in assisting TEM analyses.

Reference

1. Thevenot F. Boron carbide-a comprehensive review. *J Eur Ceram Soc* 1990;**6**:205-25.

2. Domnich V, Reynaud S, Haber R, Chhowalla M. Boron carbide: structure, properties, and stability under stress. *J Am Ceram Soc* 2011; **94**:3605-28.

3. Mashhadi M, Taheri-Nassaj E, Sglavo V, Sarpoolaky H, Ehsani N. Effect of Al addition on pressureless sintering of B_4C. *Ceram Int* 2009; **35**: 831-7.

4. Suri A, Subramanian C, Sonber J, Murthy T. Synthesis and consolidation of boron carbide: a review. *Int Mater Rev* 2010; **55**:4-39.

5. Kim H, Koh Y, Kim H. Densification and mechanical properties of B_4C with Al_2O_3 as a sintering aid. *J Am Ceram Soc* 2000; **83**: 2863-5.

6. Ye F, Hou Z, Zhang H, Liu L. Densification and mechanical properties of spark

plasma sintered B_4C with Si as a sintering aid. *J Am Ceram Soc* 2010; **93**: 2956-9.

7. Zorzi J, Perottoni C, Jornada J. Hardness and wear resistance of B_4C ceramics prepared with several additives. *Mater Lett* 2005;**59**:2932-5.

8. Levin L, Frage N, Dariel M. A novel approach for the preparation of B_4C-based cermets. *Int J Refract Met Hard Mater* 2000;**18**:131-5.

9. Srivatsan T, Guruprasad G, Black D, Radhakrishnan R, Sudarshan T. Influence of TiB_2 content on microstructure and hardness of TiB_2-B_4C composite. *Powder Technol* 2005;**159**:161-7.

10. Yamada S, Hirao K, Yamauchi Y, Kanzaki S. Densification behavior and mechanical properties of pressureless-sintered B_4C-CrB_2 ceramics. *J Mater Sci* 2002; **37**:5007-12.

11. Dole S, Prochazka S. Doremus R. Microstructural coarsening during sintering of boron carbide. *J Am Ceram Soc* 1989;**72**:958-66.

12. Schwaighofer. E, Clemens. H, Mayer. S, Lindemann. J, Klose. J, Smarsly W, Guther. V. Microstructural design and mechanical properties of a cast and heat-treated intermetallic multi-phase gamma-TiAl based alloy. *Intermetallics* 2014;**44**:128-40.

13. Schwaighofer. E, Clemens. H, Lindemann. J, Stark. A, Mayer. S. Hot-working behavior of an advanced intermetallic multi-phase gamma-TiAl based alloy. *Mat Sci Eng A-Struct* 2014;614:297-310.

14. Ji W, Rehman S, Wang W, Wang H, Wang Y, Zhang J, Zhang F, Fu Z. Sintering boron carbide ceramics without grain growth by plastic deformation as the dominant

densification mechanism. *Sci Rep* 2015;**5**:15827.

15. Hayun S, Paris V, Dariel MP, Frage N, Zaretzky E. Static and dynamic mechanical properties of boron carbide processed by spark plasma sintering. *J Eur Ceram Soc* 2009;**29**:3395-400.

16. Niihara K, Nakahira A, Hirai T. The Effect of stoichiometry on mechanical properties of boron carbide. *J Am Ceram Soc* 1984;**67**:C13-4.

17. Lee H, Speyer R. Pressureless sintering of boron carbide. *J Am Ceram Soc* 2003;**86**:1468-73.

18. Hayun S, Kalabukhov S, Ezersky V, Dariel M, Frage N. Microstructural characterization of spark plasma sintered boron carbide ceramics. *Ceram Int* 2010; **36**: 451-7.

19. Shen Z, Peng H, Liu J, Nygren M. Conversion from nano- to micron-sized structures: experimental observations. *J Eur Ceram Soc* 2004;**24**:3447-52.

20. Ji W, Zhang J, Wang W, Wang H, Zhang F, Wang Y, Fu Z. Fabrication and properties of TiB_2-based cermets by spark plasma sintering with CoCrFeNiTiAl High-entropy Alloy as sintering aid. *J Eur Ceram Soc* 2015;**35**:879-86.

Table Captions

Table 1

Comparison of the properties in the present work with other B_4C-based ceramics.

Table 1. Comparison of the properties in the present work with other B_4C-based ceramics

Material (wt. %)	Processing	Relatively density (%)	Flexural strength (MPa)	Vickers hardness (GPa)	Fracture toughness ($MPa \cdot m^{0.5}$)	Reference
Pure B_4C	HP, 2150 °C, 36 MPa, 60 min	95.5	300-400	32.5	2.5-3.0	[4]
B_4C-TiO_2-C	HP, 2100 °C, 35 MPa, 65 min	>95	350	30	4.0	[4]
B_4C-5 Al_2O_3	HP, 2150 °C, 35 MPa, 65 min	95.5	300	22.4	3.2	[4]
Pure B_4C	SPS, 2200 °C, 32 MPa, 10 min	fully	430±21	32±2	3.9-4.9	[15]
B_4C-5 Al_2O_3	SPS, 1800 °C, 50 MPa, 5 min	97.1	-	29.35±0.17	2.98±0.76	[23]
B_4C-5 Ti-Al intermetallics	SPS, 1700 °C, 32 MPa, 5 min	99.5	506±14	33.5±0.4	5.5±0.1	Present work

Figure 1

Click here to download high resolution image

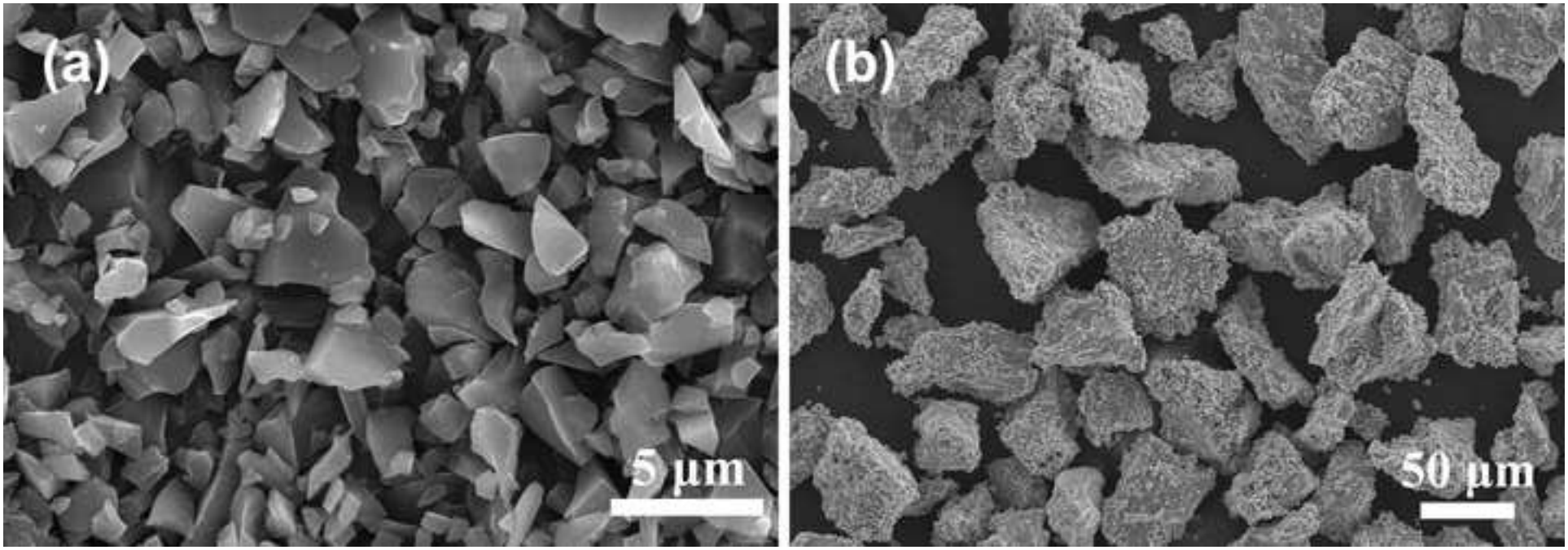

Figure 2

Click here to download high resolution image

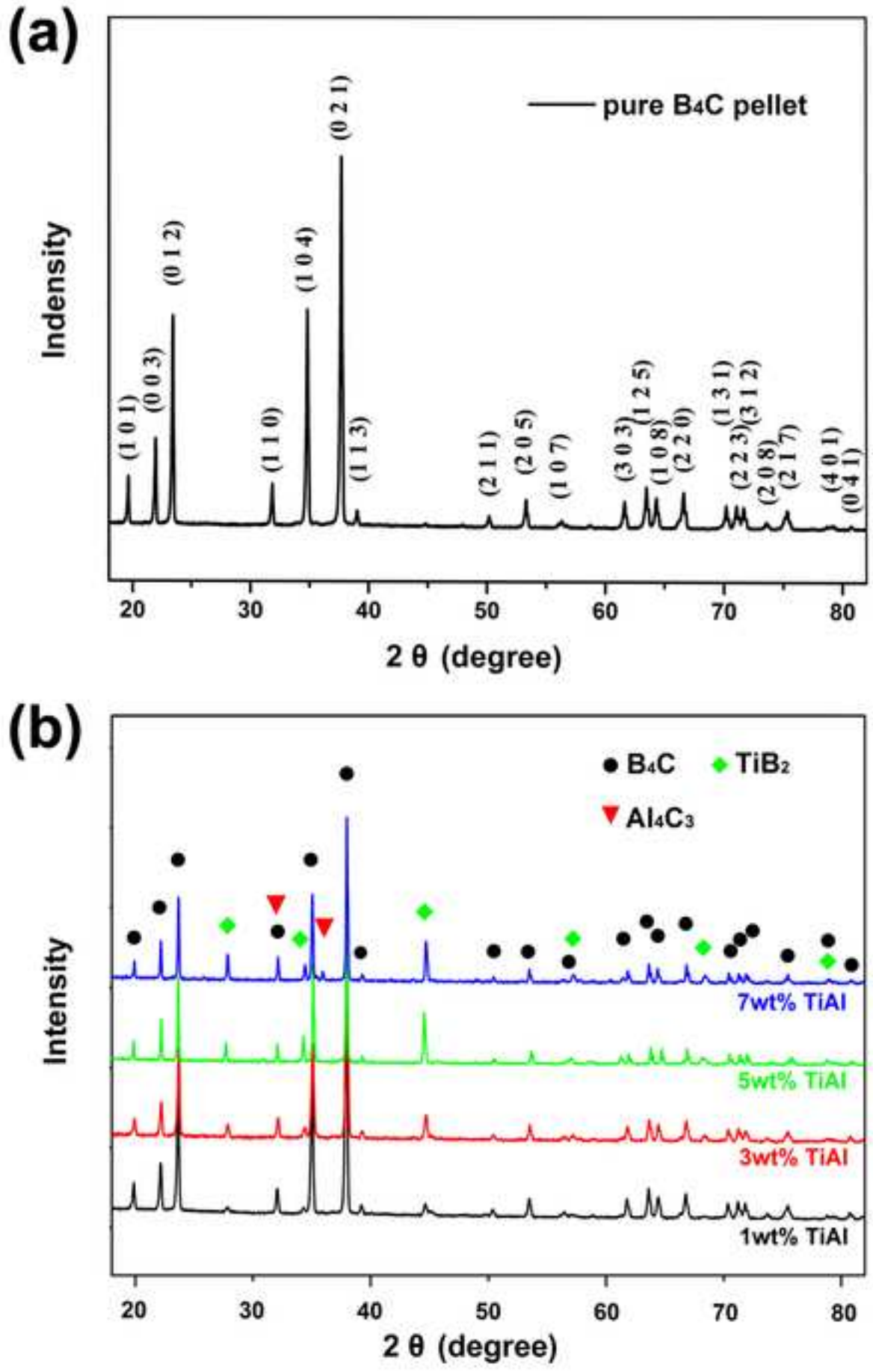

Figure 3(a)
Click here to download high resolution image

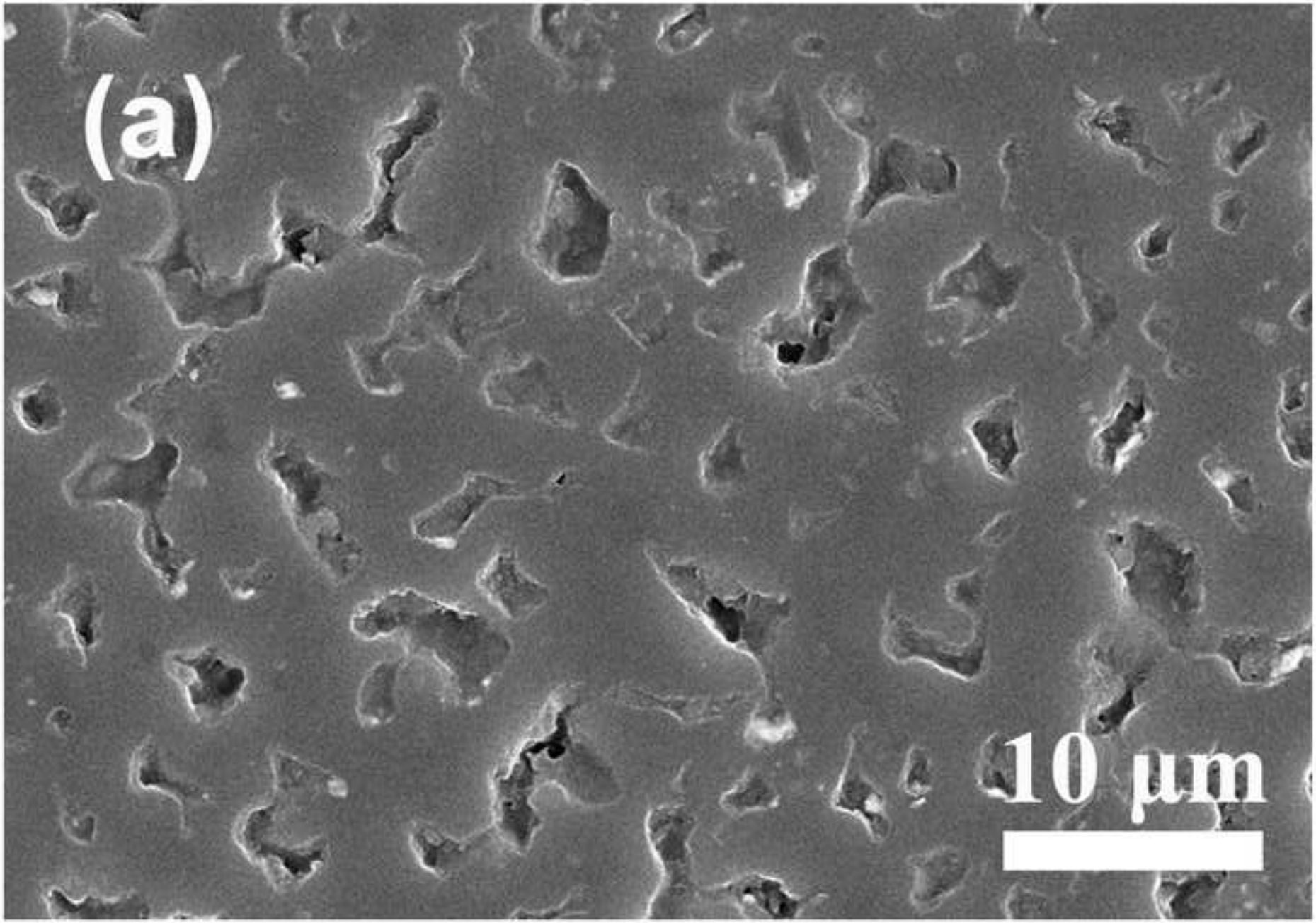

Figure 3(b)
Click here to download high resolution image

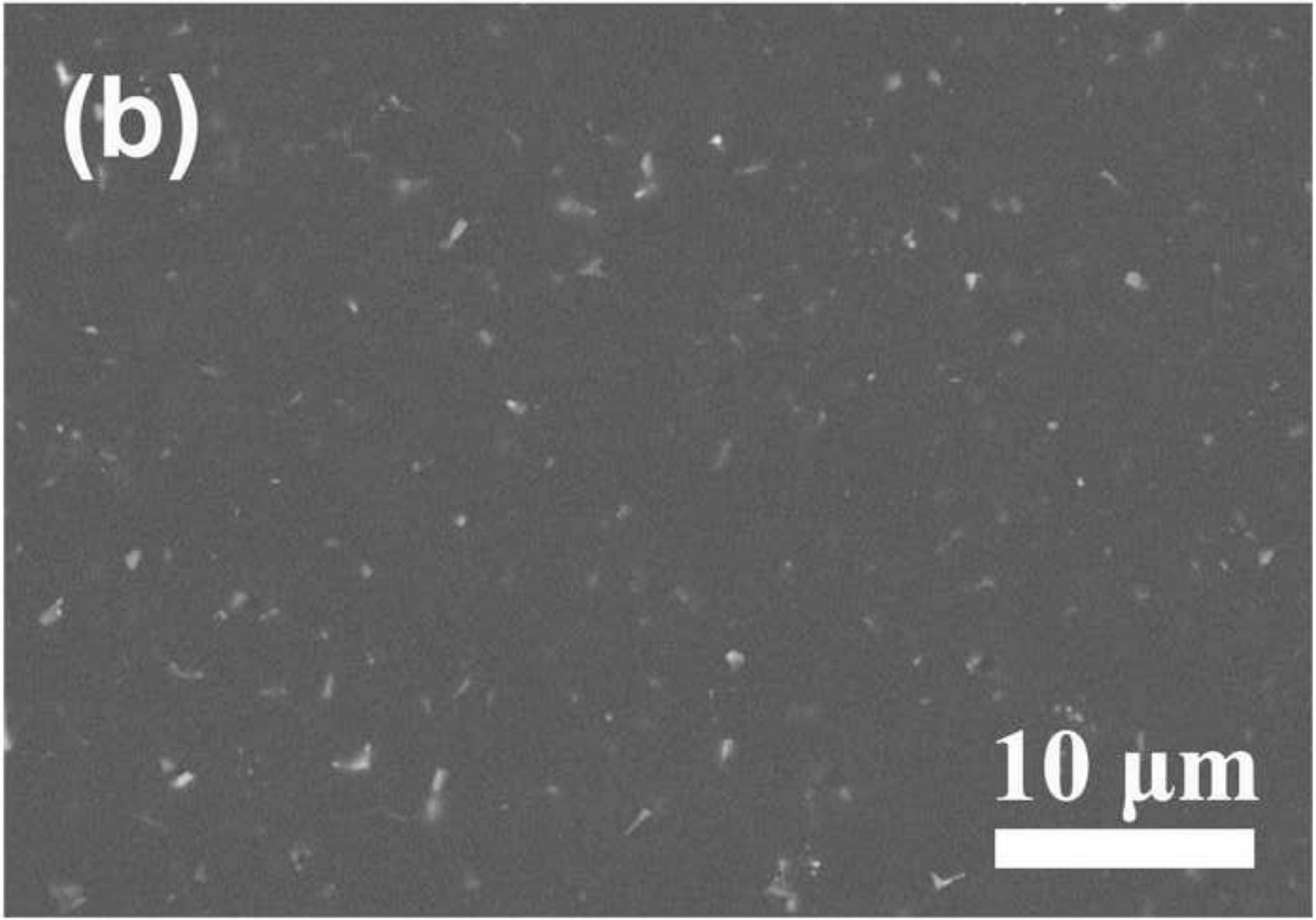

Figure 3(c)
Click here to download high resolution image

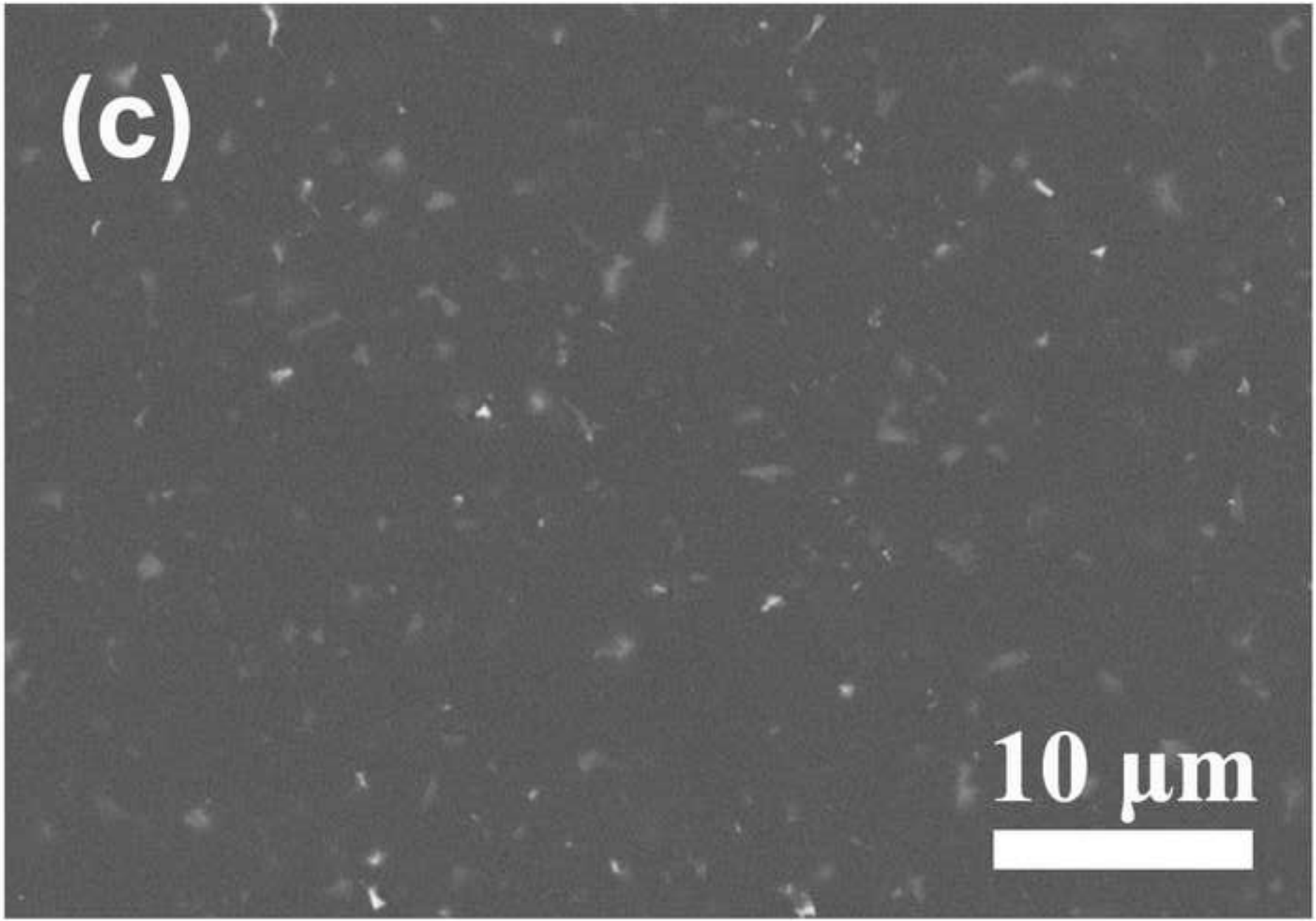

Figure 3(d)
Click here to download high resolution image

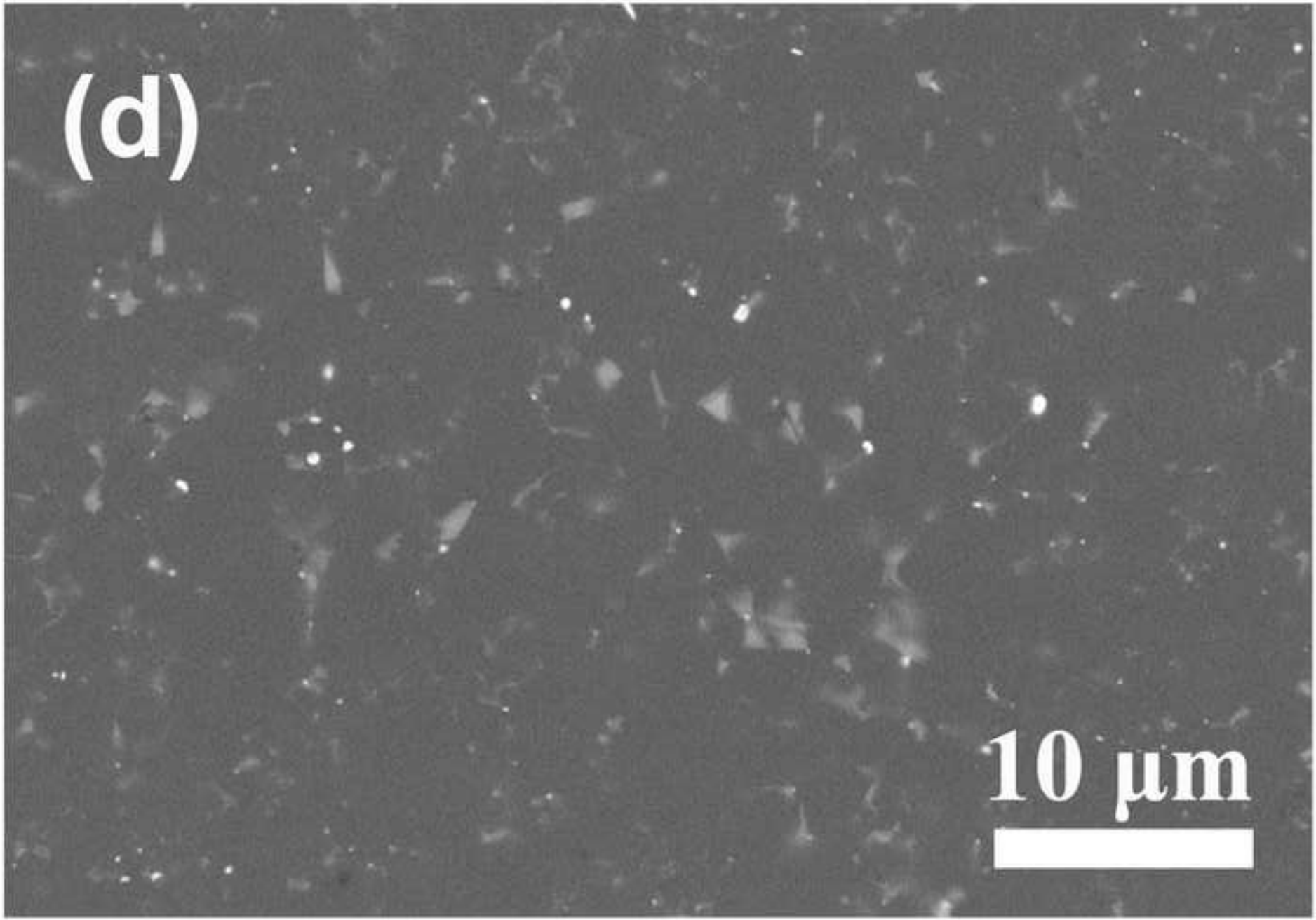

Figure 3(e)
Click here to download high resolution image

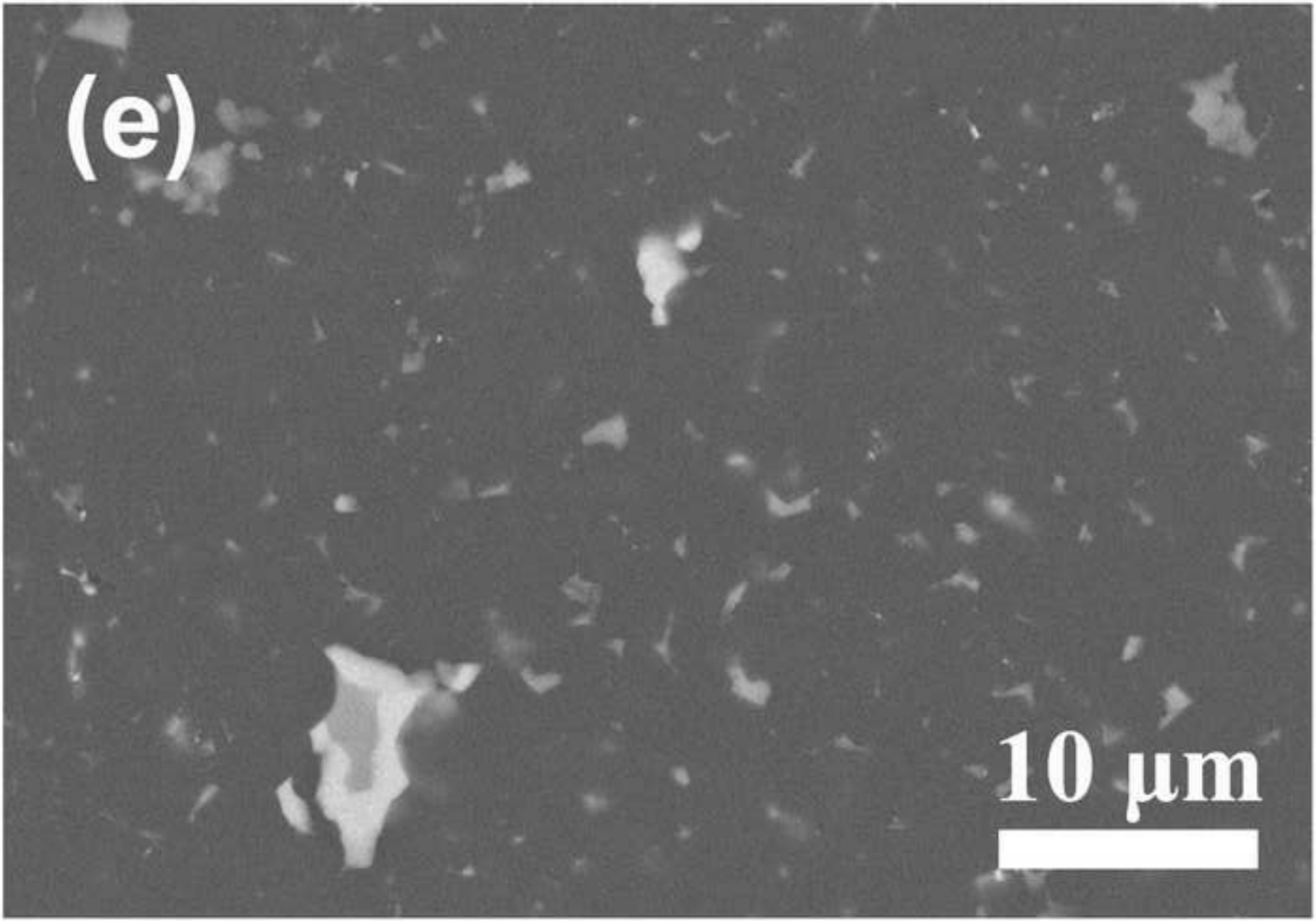

Figure 3(f)
Click here to download high resolution image

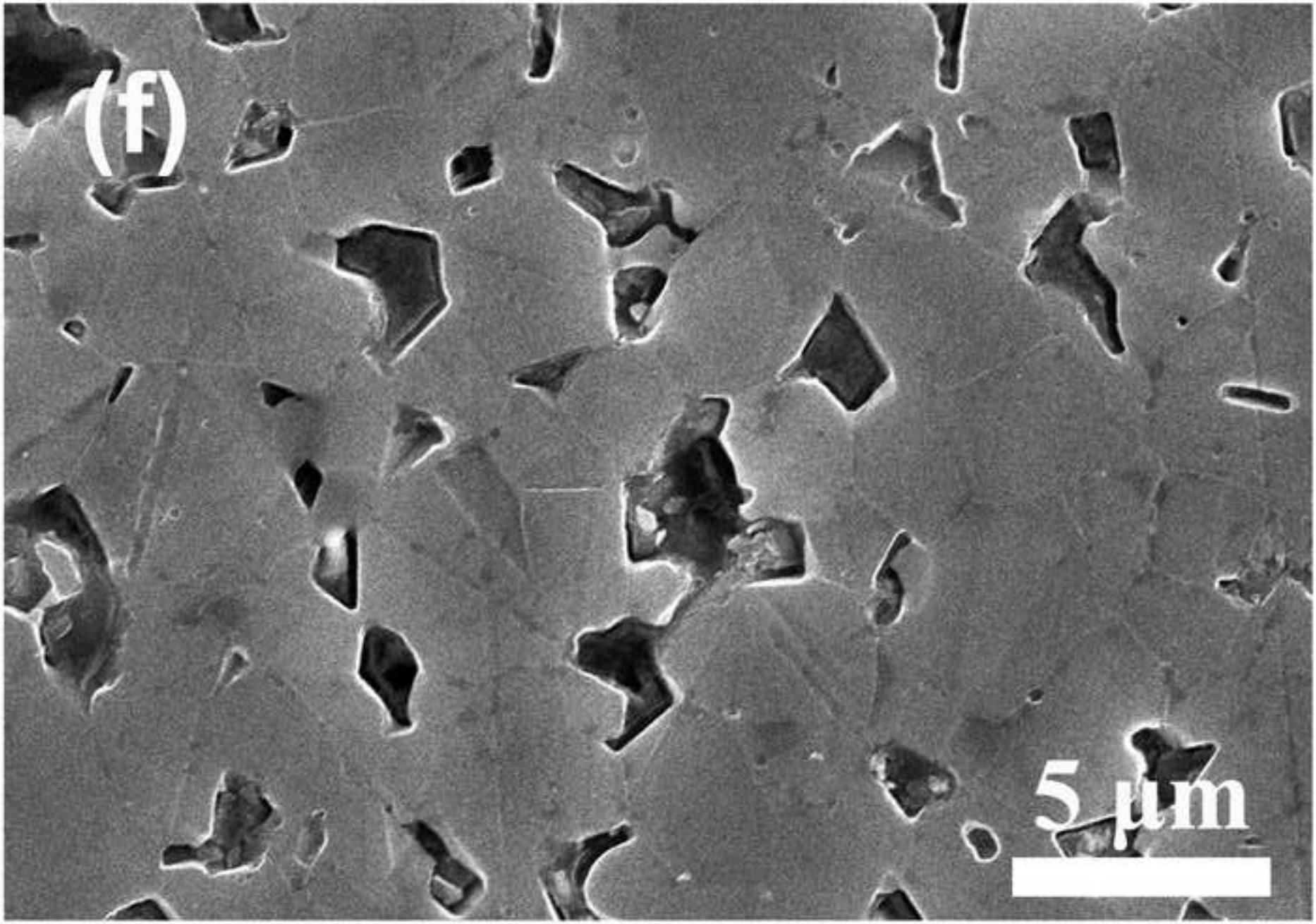

Figure 3(g)
Click here to download high resolution image

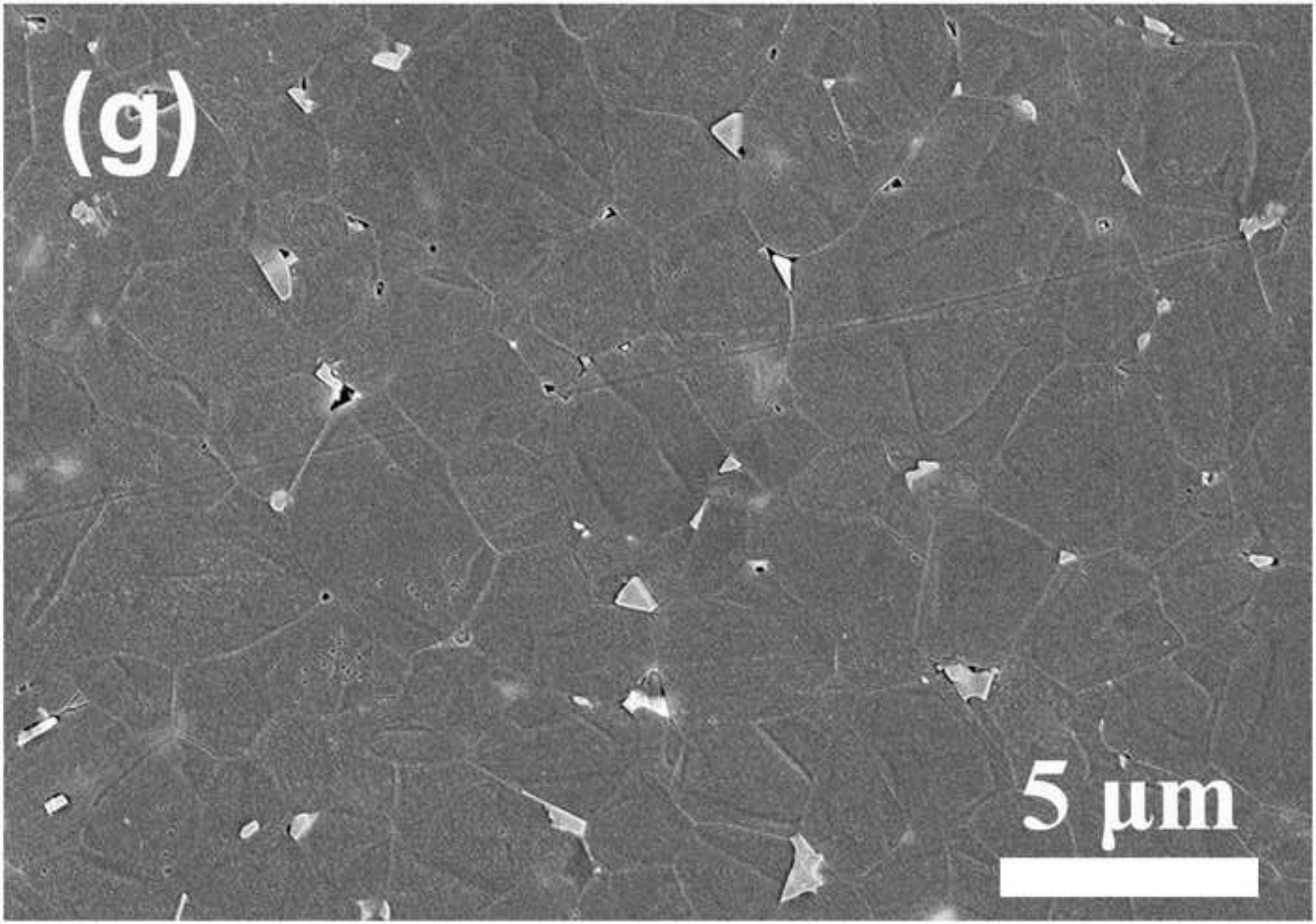

Figure 3(h)

Click here to download high resolution image

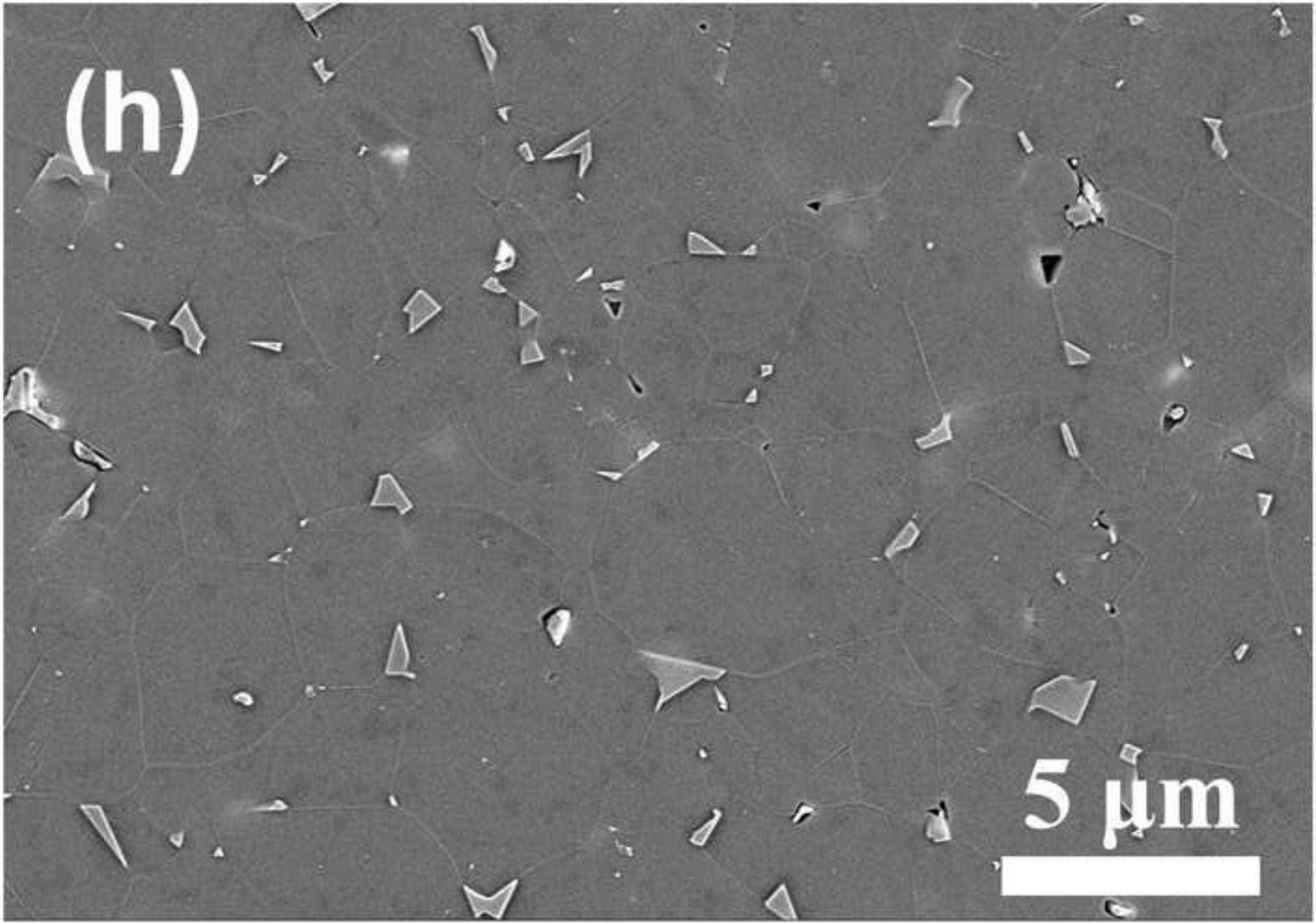

Figure 3(i)

Click here to download high resolution image

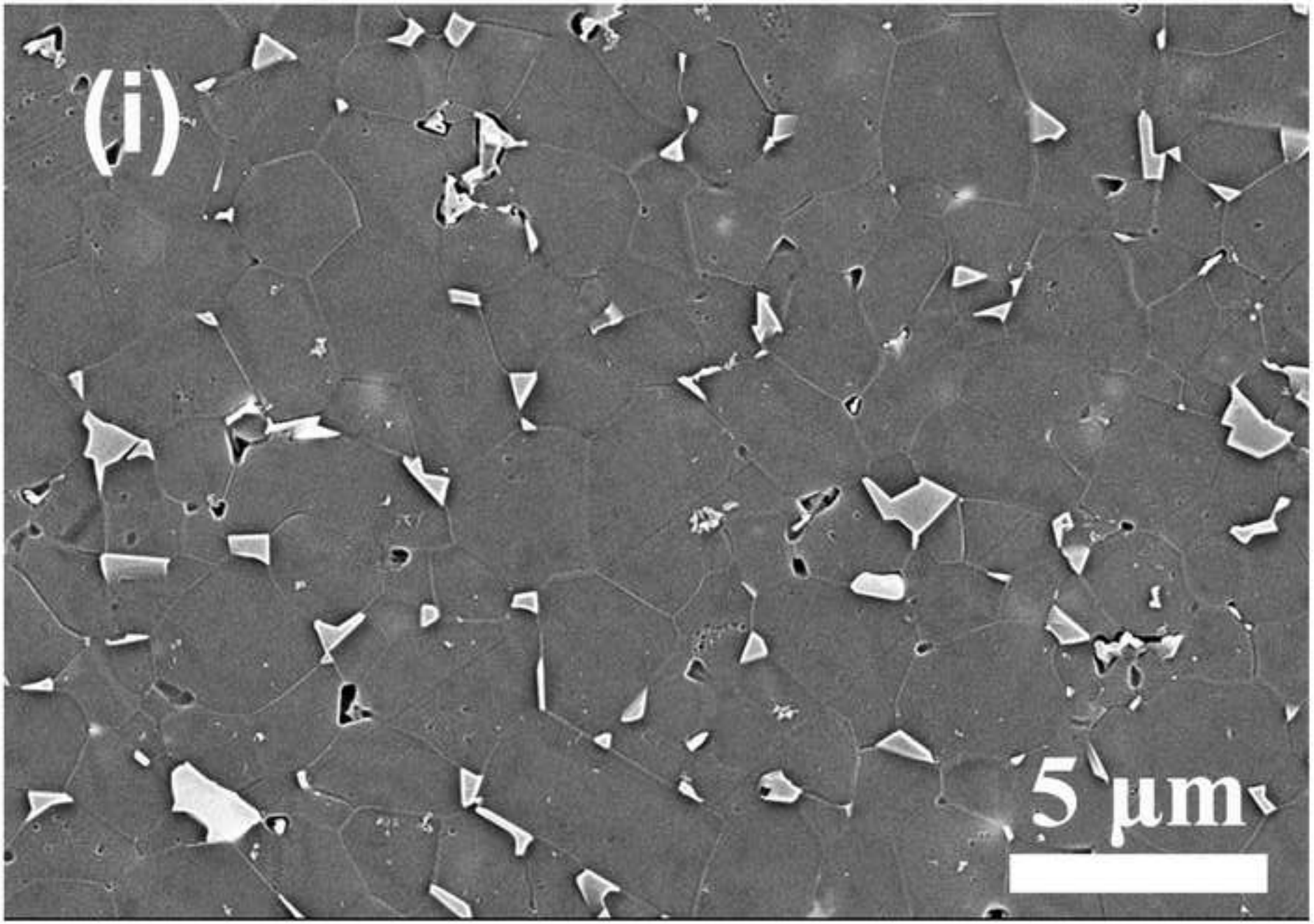

Figure 3(j)

Click here to download high resolution image

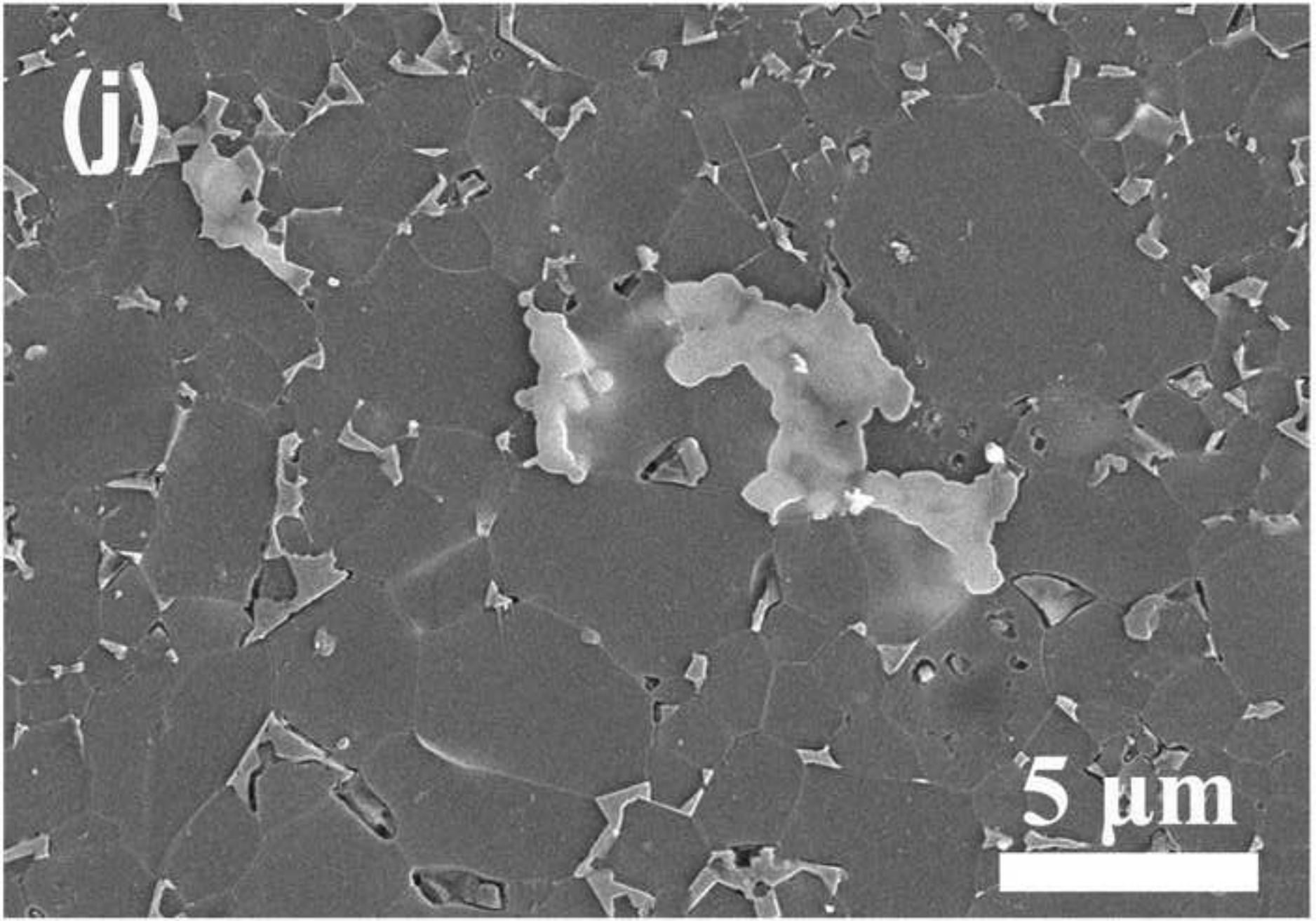

Figure 4

Click here to download high resolution image

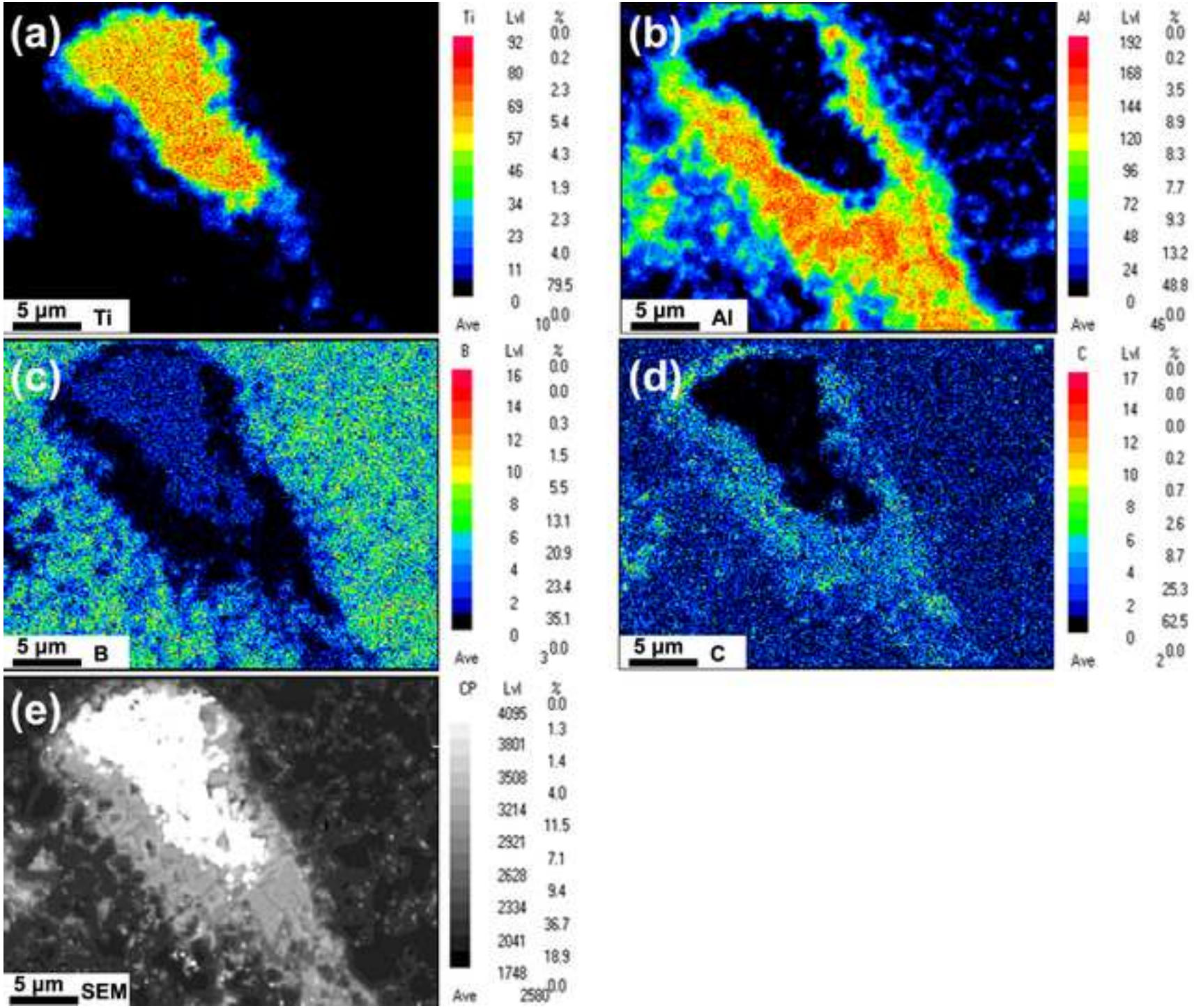

Figure 5

Click here to download high resolution image

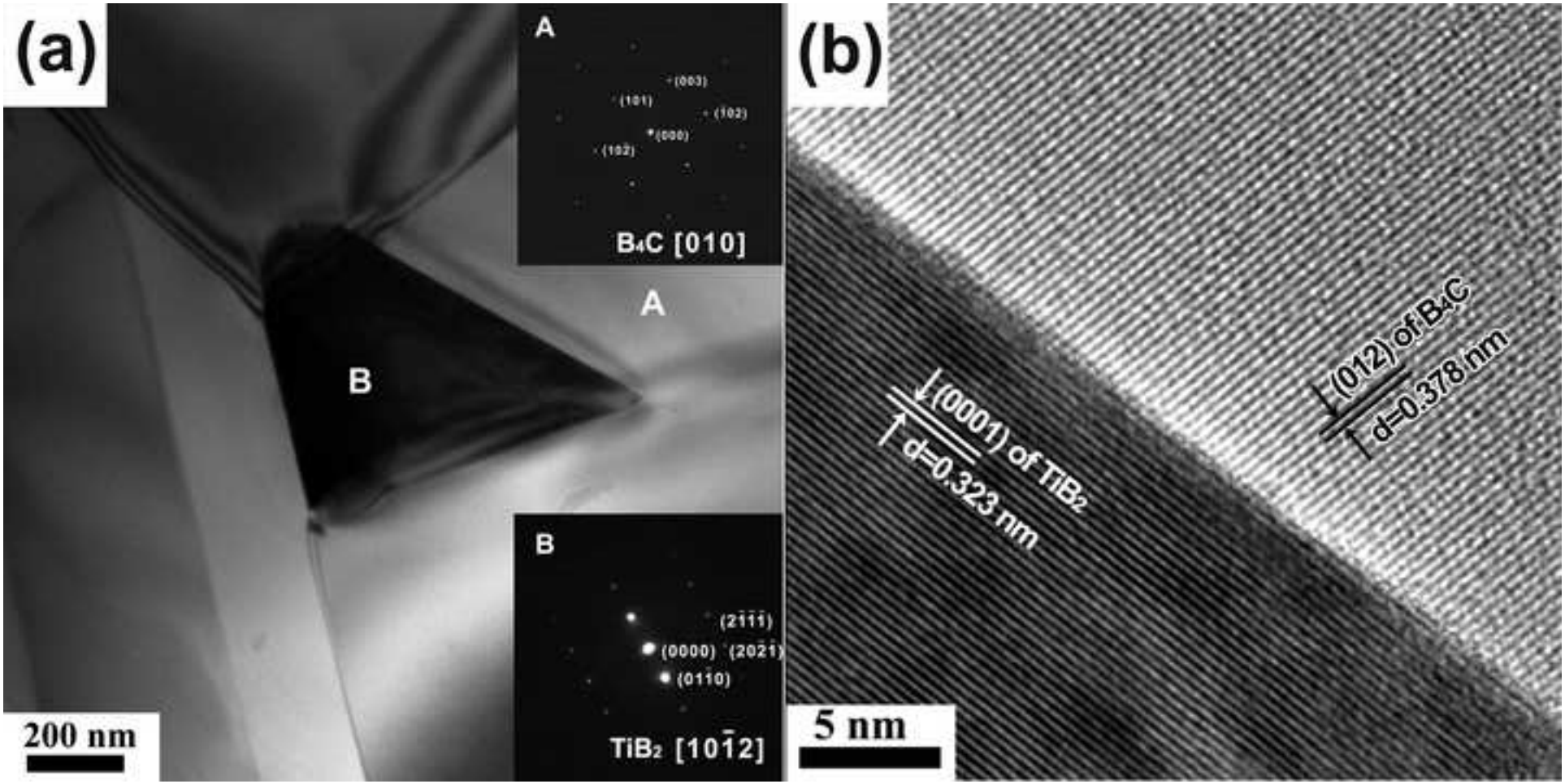

Figure 6

Click here to download high resolution image

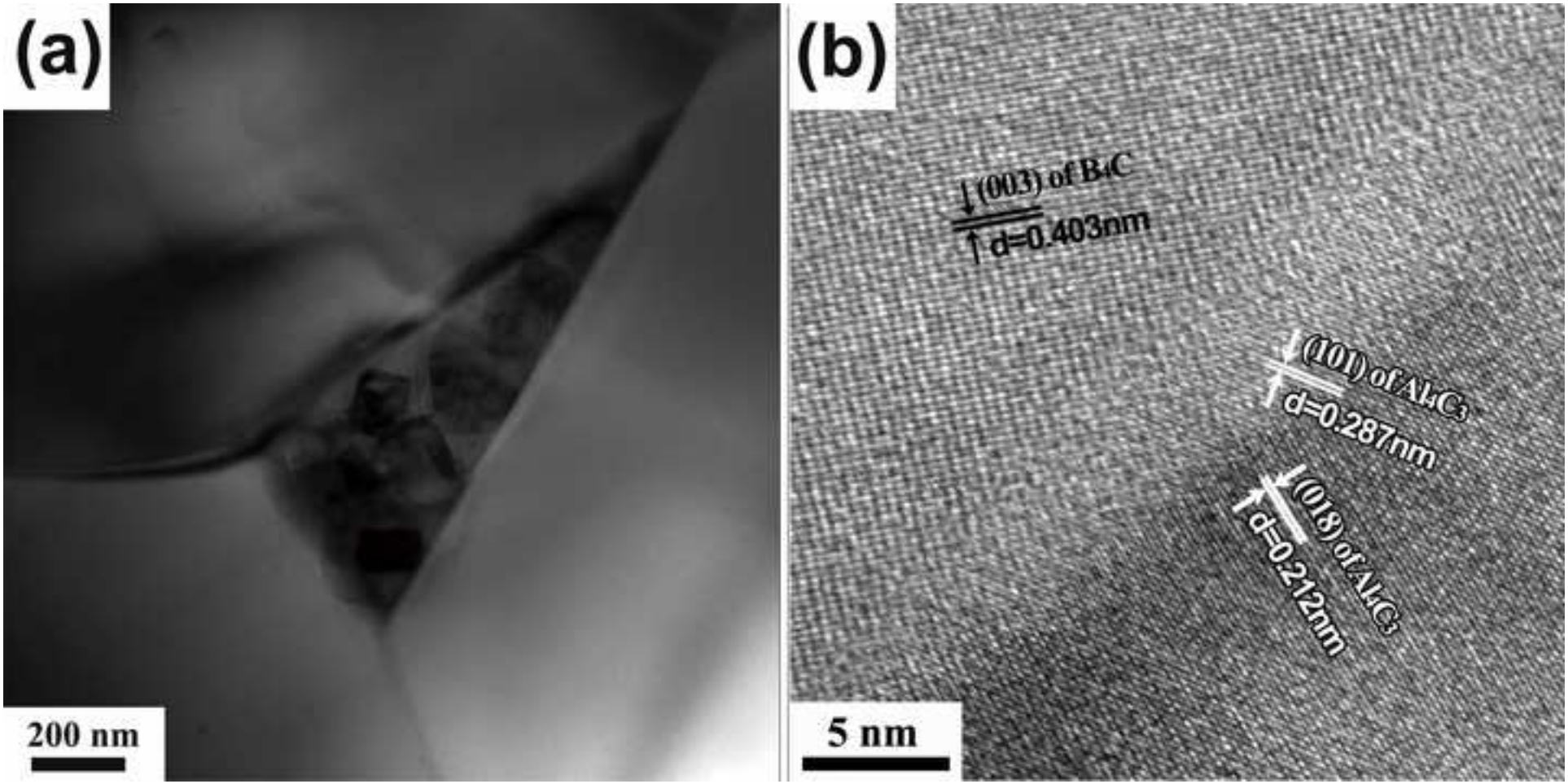

Figure 7

Click here to download high resolution image

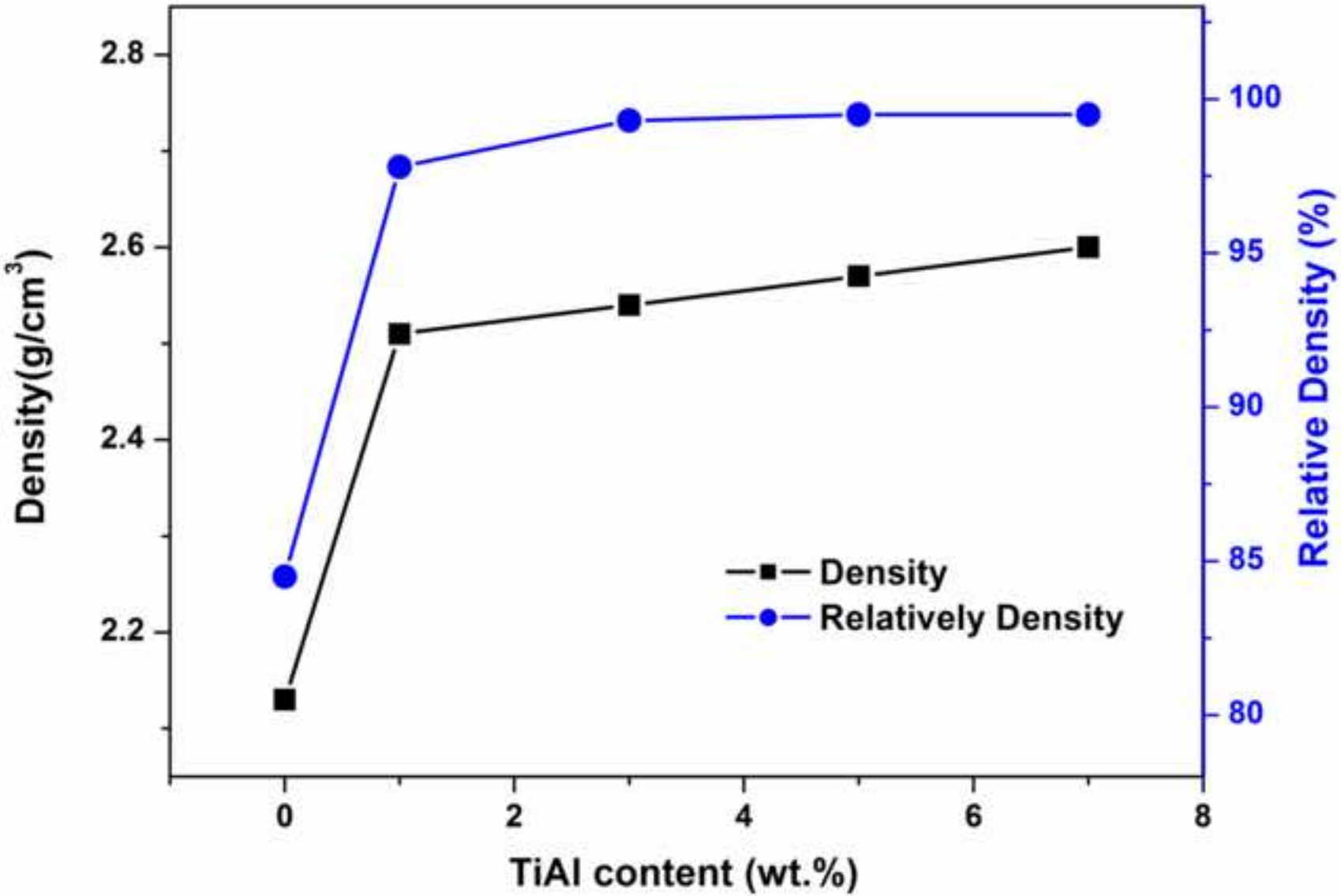

Figure 8

Click here to download high resolution image

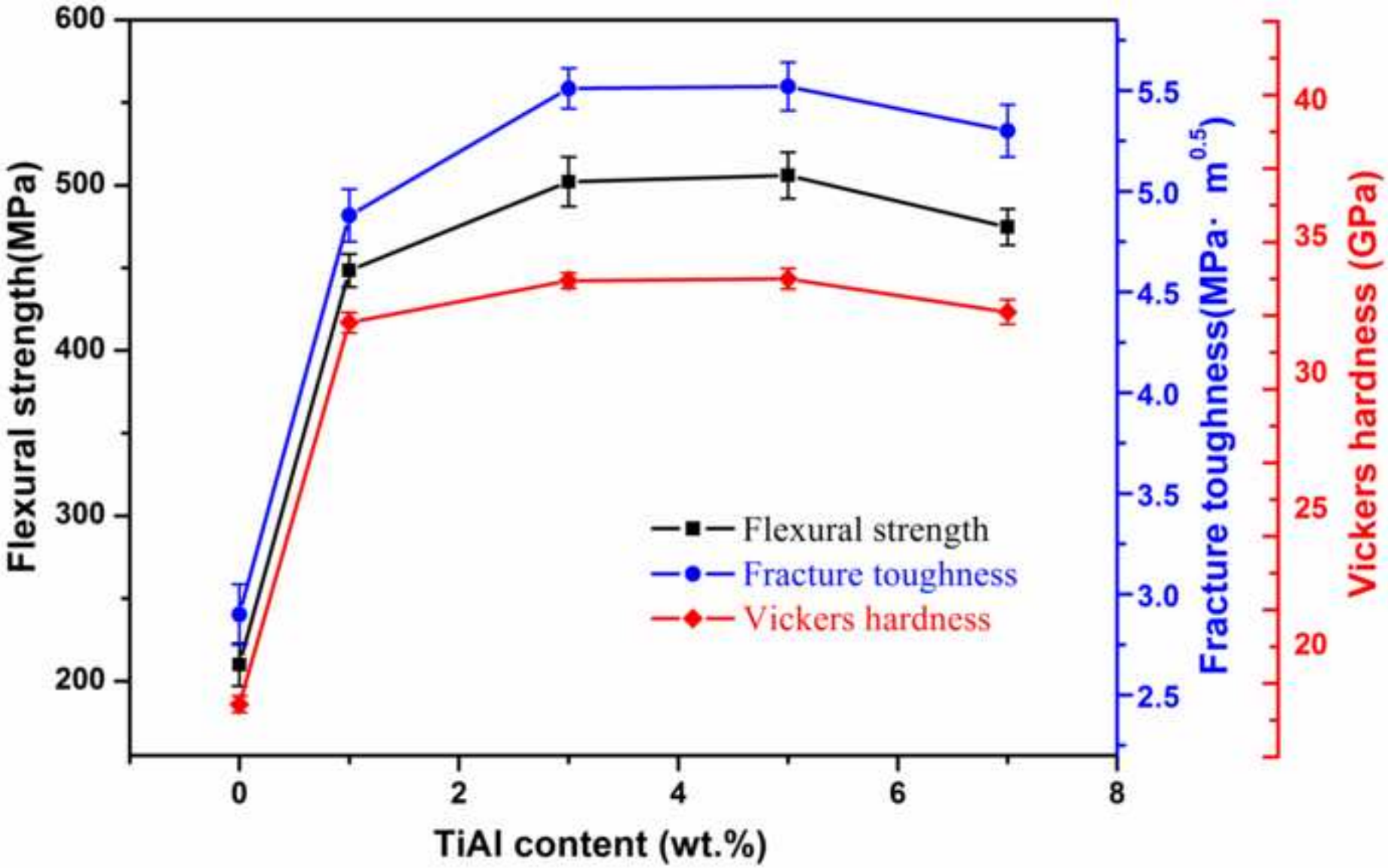

Figure 9
Click here to download high resolution image

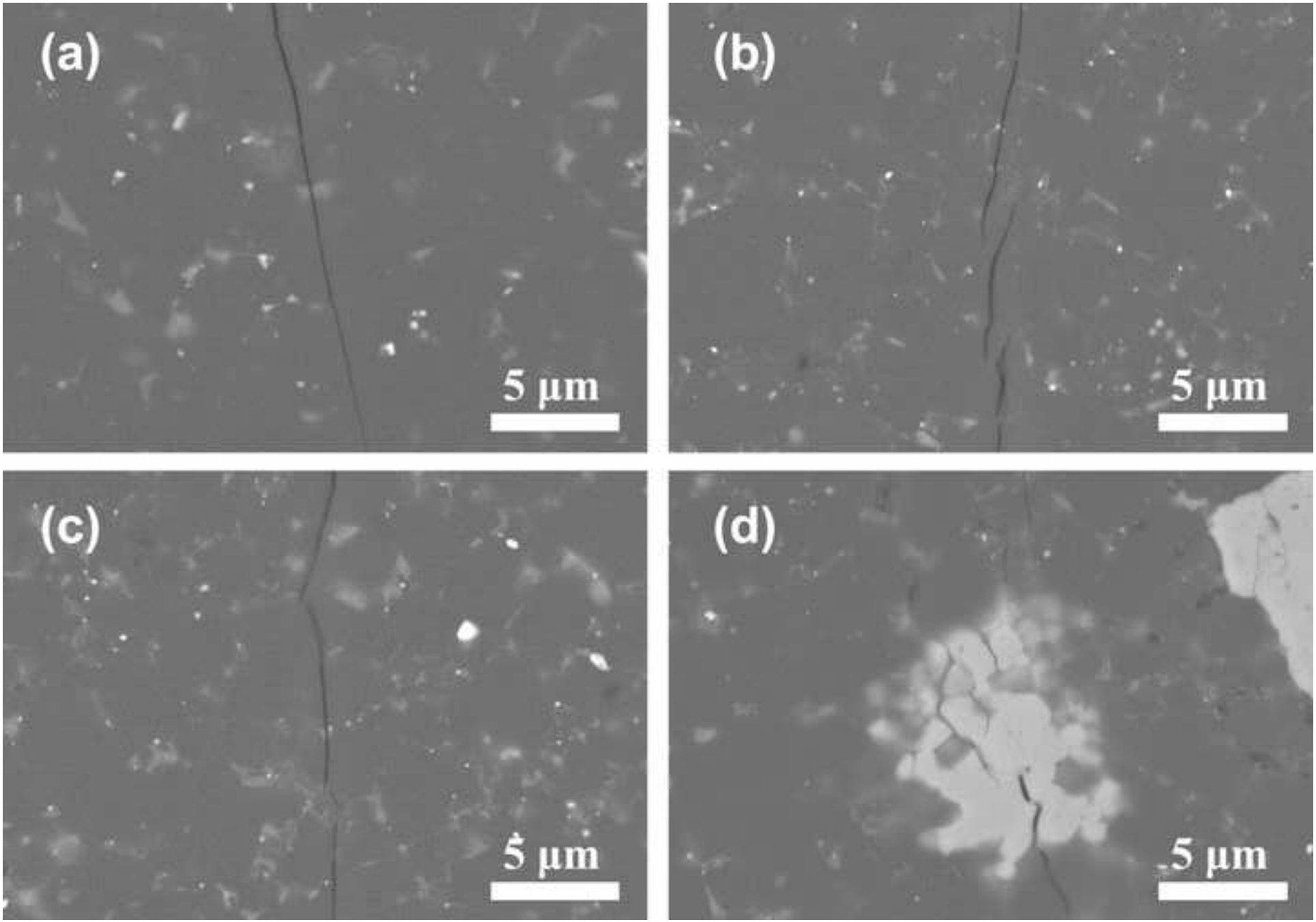

Figure Captions

Fig. 1. SEM images of raw material: (a) B_4C ceramic powder; (b) Ti-Al intermetallic powder.

Fig. 2. XRD patterns of B_4C-based ceramics with the addition of Ti-Al intermetallics from 0 to 7 wt. %.

Fig. 3. Polished and electrochemically etched surfaces of B_4C-based ceramics with the addition of Ti-Al from 0 to 7 wt. %. (a)-(e) polished surfaces: (a) pure B_4C sample ; (b) 1 wt. % Ti-Al addition; (c) 3 wt. % Ti-Al addition; (d) 5 wt. % Ti-Al addition; (e) 7 wt. % Ti-Al addition; (f)-(j) etched surfaces: (f) pure B_4C sample ; (g) 1 wt. % Ti-Al addition; (h) 3 wt. % Ti-Al addition; (i) 5 wt. % Ti-Al addition; (j) 7 wt. % Ti-Al addition.

Fig. 4. EPMA mapping of the B_4C-based ceramics with 7 wt. % Ti-Al intermetallics: (a)-(d) The elemental distribution maps of Ti, Al, B and C and (e) Backscattering image.

Fig. 5. TEM images of the morphology and grain boundary structure between B_4C and TiB_2.

Fig. 6. TEM images of the morphology and grain boundary structure between B_4C and Al_4C_3.

Fig. 7. The density and relative density of the B_4C-based ceramics with different addition of Ti-Al intermetallics.

Fig. 8. The flexural strength, fracture toughness and Vickers hardness of the B_4C-based ceramics with different additions of Ti-Al intermetallics.

Fig. 9. The SEM images of the crack propagating after indentation on the polished surface of B_4C ceramics with different Ti-Al intermetallic additions: (a) 1 wt. % Ti-Al addition; (b) 3 wt. % Ti-Al addition; (c) 5 wt. % Ti-Al addition; (d) 7 wt. % Ti-Al.